ACS APPLIED MATERIALS & INTERFACES

Research Article

Cite This: ACS Appl. Mater. Interfaces 2018, 10, 33441−33449

www.acsami.org

Deep UV Emission from Highly Ordered AlGaN/AlN Core−Shell Nanorods

Pierre-Marie Coulon,*[,†] Gunnar Kusch,[‡] Robert W. Martin,[‡] and Philip A. Shields[†]

[†]Department of Electronic and Electrical Engineering, Centre of Nanoscience & Nanotechnology, University of Bath, Bath BA2 7AY, U.K.

[‡]Department of Physics, SUPA, University of Strathclyde, Glasgow G4 0NG, U.K.

Supporting Information

ABSTRACT: Three-dimensional core−shell nanostructures could resolve key problems existing in conventional planar deep UV light-emitting diode (LED) technology due to their high structural quality, high-quality nonpolar growth leading to a reduced quantum-confined Stark effect and their ability to improve light extraction. Currently, a major hurdle to their implementation in UV LEDs is the difficulty of growing such nanostructures from $Al_xGa_{1-x}N$ materials with a bottom-up approach. In this paper, we report the successful fabrication of an $AlN/Al_xGa_{1-x}N/AlN$ core−shell structure using an original hybrid top-down/bottom-up approach, thus representing a breakthrough in applying core−shell architecture to deep UV emission. Various $AlN/Al_xGa_{1-x}N/AlN$ core−shell structures were grown on optimized AlN nanorod arrays. These were created using displacement Talbot lithography (DTL), a two-step dry-wet etching process, and optimized AlN metal organic vapor phase epitaxy regrowth conditions to achieve the facet recovery of straight and smooth AlN nonpolar facets, a necessary requirement for subsequent growth. Cathodoluminescence hyperspectral imaging of the emission characteristics revealed that 229 nm deep UV emission was achieved from the highly uniform array of core−shell $AlN/Al_xGa_{1-x}N/AlN$ structures, which represents the shortest wavelength achieved so far with a core−shell architecture. This hybrid top-down/bottom-up approach represents a major advance for the fabrication of deep UV LEDs based on core−shell nanostructures.

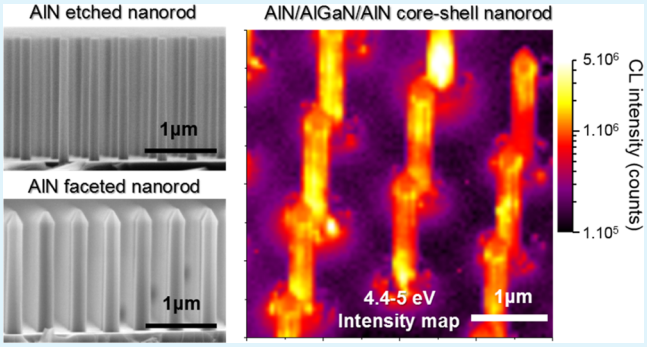

KEYWORDS: *nanorod, core−shell, AlN, AlGaN, TEM, EDX, cathodoluminescence*

It is well-known that the III-nitride semiconductors are an important class of materials for devices emitting in the ultraviolet (UV) with applications, including UV curing,[1] medical diagnostics, phototherapy,[2] optical sensing,[3] security, communications,[4] sterilization, and water and air purification.[5−7] These applications are made possible thanks to the widely tunable bandgap energy of AlGaN alloys ranging from 3.4 eV for GaN to 6.2 eV for AlN. The emission wavelength of AlGaN-based light-emitting diodes (LEDs) can cover the entire UV-A, UV-B, and UV-C spectral range. This represents one of the major advantages compared to the mercury lamps and gas lasers that possess a fixed and limited emission spectrum. Additionally, III-nitride UV-based LEDs and LDs are compact, robust, environmentally friendly, offer a long lifetime and have a considerably lower power requirement. However, although visible white-light LEDs based on indium-containing III-nitrides are today sufficiently efficient and cheap to be established as the leading technology for public and home lighting, UV LEDs still require substantial improvements. Currently, the external quantum efficiency (EQE) of $Al_xGa_{1-x}N$ LEDs barely reaches a maximum of 40% in the UV-A,[8] 20% in the UV-B,[9] and up to a few percent in the deep UV-C.[8,10] This is significantly lower than the 80% EQE achieved for GaN-based blue LEDs.[11,12] This gap in terms of efficiency between deep UV and visible LEDs is due to several factors, such as the high density of point and extended defects, which can act as nonradiative recombination centers in AlN and $Al_xGa_{1-x}N$ materials,[13,14] the low-carrier injection and difficulties in achieving efficient p-doping in AlN-rich $Al_xGa_{1-x}N$ alloys,[15,16] the poor light extraction,[17−19] and the internal electric field in quantum wells,[20,21] which are exacerbated compared to GaN due to the much larger spontaneous polarization properties of AlN-based materials.[22]

In a large part, these challenges result directly from the approach employed to fabricate these LEDs, which is now-a-days based on a planar technology. The use of three-dimensional (3D) nanostructures is an approach to address and mitigate some of these challenges. In particular, the use of nanorod arrays can allow the reduction of extended defects compared to those in the initial planar template by means of

Received: June 25, 2018
Accepted: September 6, 2018
Published: September 6, 2018

DOI: 10.1021/acsami.8b10605
ACS Appl. Mater. Interfaces 2018, 10, 33441−33449

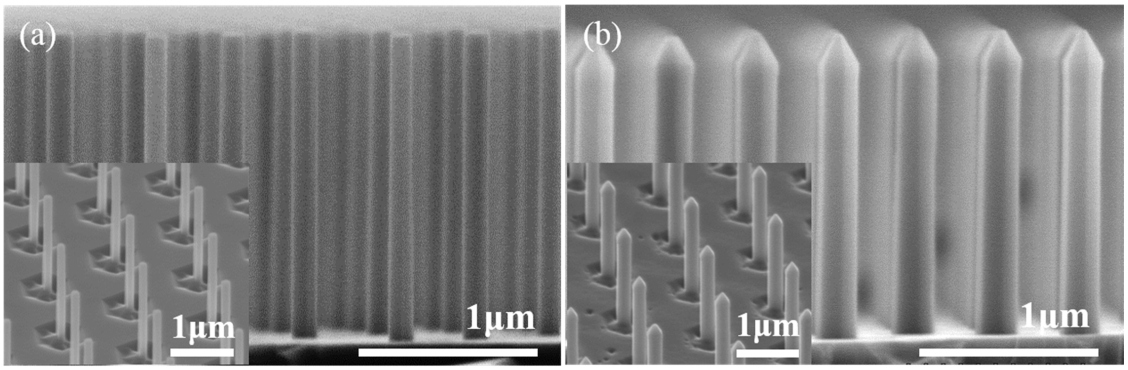

Figure 1. Cross-section SEM images of (a) AlN nanorod arrays after ICP dry etching and AZ 400K wet etching and (b) AlN-faceted nanorod arrays after MOVPE regrowth. The insets in (a) and (b) show a tilted view of the AlN-etched and -faceted nanorods, respectively.

dislocation bending[23] or filtering,[24,25] thus reducing the threading dislocations (TDs) density in the active region. Furthermore, a core−shell nanostructure configuration, with the core along the *c*-direction, involves radial growth of the quantum wells (QWs) on nonpolar facets where strong spontaneous and piezoelectric polarization are absent.[26] The mitigation of the quantum-confined Stark effect will improve the overlap between electron and hole wave functions and thus the emission efficiency. Additionally, high densities of basal-plane stacking faults (BSFs) have been observed in planar nonpolar AlGaN layers,[27] since BSFs can effectively compensate lattice translations between islands that occur during the early stage of heteroepitaxial growth.[28] In contrast, nanostructures aligned along the *c*-direction are formed from growth in the polar direction, for which BSFs are not observed away from the substrate interface. Therefore, the nonpolar sidewalls of core−shell nanostructures offer the prospect of a higher structural quality for the QWs and hence an increase in the internal quantum efficiency (IQE). Moreover, the QW growth, occurring radially to the nanorod core, can dramatically increase the overall emitting area over that of a planar equivalent.[29] Such a benefit is important because poor efficiency in nitride LEDs at high current injection occurs at high carrier densities. Spreading a high current over the larger emissive surface area of core−shell structures brings the device back into its high-efficiency, low-carrier density regime.[30] Finally, the use of nanostructures also improves the light extraction efficiency of the devices, for example, by randomizing the angular distribution of the photons in the LED.[31,32]

However, a key obstacle to the implementation of core−shell structures in UV devices is the difficulty of growing such regular structures in $Al_xGa_{1-x}N$-based materials. Whereas the selective area growth (SAG) of GaN nanorod arrays and subsequent InGaN/GaN-based core−shell LEDs has been demonstrated by metal organic vapor phase epitaxy (MOVPE),[33−36] the SAG of AlN and Al-rich AlGaN nanorods has not been achieved yet due to the very high sticking coefficient and the low diffusion length of Al atoms.[37,38] A recent report of AlGaN nanorods by molecular beam epitaxy (MBE) on a Si substrate[39] shows how AlGaN nanostructures could be used to circumvent the challenges of planar technology. However, they require a GaN pedestal grown on Si to initiate the nucleation.[39−41] Ultimately, sapphire substrates and GaN-free structures are required for devices operating in the UV-C regime to avoid absorption of the UV-C light. Additionally, MBE-based nanorods have, up to now, only been demonstrated to be suitable for the growth of axial structures and not core−shell structures, which provide larger active areas. The recent report of Kim et al. represents the only success to date to create an AlGaN/AlN core−shell structure.[42] They report the fabrication of AlN nanorods on a sapphire substrate by polarity-selective epitaxy and etching and achieved 260 nm emission from core−shell MQWs. Their results further highlight the potential of the core−shell geometry with an improved PL intensity and IQE of the MQW over one grown on planar AlN. However, their approach is based on the use of Al-polar AlN inversion domains to create the core, which leads to irregular and unorganized structures; unsuitable for real devices. An alternative route, already demonstrated for InGaN/GaN core−shell nanorod arrays,[43−45] uses top-down etching followed by MOVPE regrowth. It is a promising route for the fabrication of uniform and highly organized AlN nanorod arrays that will subsequently allow the creation of AlGaN/AlN core−shell devices.[46,47] We have recently demonstrated this first critical step prior to creating device structures with active quantum wells.[38]

In this paper, we present uniform and organized core−shell AlN/AlGaN/AlN nanorod arrays with a vertical nonpolar AlGaN/AlN single QW, using this hybrid top-down/bottom-up approach. The emission characteristics of the AlGaN/AlN QW are studied in detail by cathodoluminescence (CL) hyperspectral imaging. Uniform emission from the nonpolar facets is tuned to cover the UV-C spectral range from 265 to 229 nm, which represents the shortest wavelength achieved so far with a core−shell architecture. The results show the potential of the hybrid top-down/bottom-up approach to achieve nonpolar core−shell AlGaN/AlN nanorod arrays on a wafer scale to achieve deep UV light-emitting devices.

RESULTS AND DISCUSSION

The AlGaN/AlN nonpolar core−shell nanorod array was fabricated using a hybrid approach composed of top-down etching and subsequent bottom-up MOVPE regrowth. To create the AlN nanorod cores, a ∼4−5 μm AlN template grown by MOVPE on (0001) sapphire substrates was employed. We used displacement Talbot lithography (DTL) to fabricate a metal dot mask via a lift-off process, in a similar way to our previous work.[38,47] A detailed description of the DTL patterning and lift-off process is presented in the Methods section. This fast and robust fabrication process, performed on a full 2 inch wafer, allows the creation of a hexagonal array of metal dots with a diameter of ∼250 nm and a pitch of 1.5 μm, as shown in Figure S2.

DOI: 10.1021/acsami.8b10605
ACS Appl. Mater. Interfaces 2018, 10, 33441−33449

Inductively coupled plasma (ICP) etching with a chlorine chemistry was then used to transfer the metal mask into the 2 inch AlN template, following the optimum etching conditions presented in our previous work and detailed in the Methods section.[38,47] A potassium hydroxide (KOH)-based wet etching was then applied by soaking the wafer in AZ 400K at 20 °C. Figure 1a shows a scanning electron microscopy (SEM) image of the resulting smooth and straight sidewalls created after both the dry and wet etching processes. This is further evidenced by transmission electron microscopy (TEM) observation on scratched AlN-etched nanorods in Figures 2a

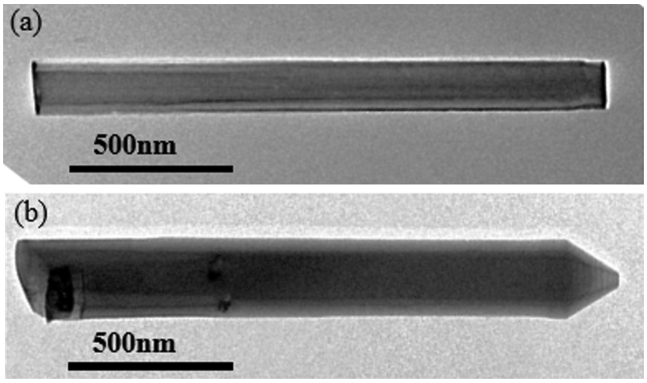

Figure 2. TEM images of scratched (a) AlN nanorod arrays after ICP dry etching and AZ 400K wet etching and (b) AlN-faceted nanorod arrays after MOVPE regrowth.

and S4. AlN nanorods with a diameter of ∼130 nm and a height of 1.8 μm were achieved. Note, the wet etching step reduces the nanorod diameter from that obtained after dry etching (Figure S3). AZ 400K solution was chosen as an etchant due to its low concentration of KOH, allowing a better control of the structure shape and etch rate. Note that similar wet etch chemistry has been used to control the dimensions of dry-etched GaN nanorods,[48] although AlN and GaN have different chemical reactivities.

Subsequently, the AlN nanorod scaffold was placed in a MOVPE reactor for the regrowth of AlN facets, at 1100 °C, 20 mbar, a V/III ratio of 30 554 and with H_2 as the carrier gas.[38,47] More details are given in the Methods section. Figure 1b demonstrates that AlN regrowth has been achieved along the whole height of the nanorod. Well-defined *m*-plane facets are formed along the nanorod sidewall together with a truncated pyramid on the top composed of six (10−11) semipolar planes and a top *c*-plane. In contrast to previous reports of AlN regrowth on etched nanorods,[46,47] straight and smooth nonpolar sidewall facets are achieved. Further evidence from TEM observations on scratched AlN-faceted nanorods can be found in Figures 2b and S5. An *m*-plane growth rate of ∼1 nm/min was extracted from SEM and TEM observations before and after regrowth.

This significant advance results from the choice of AlN regrowth conditions and the initial morphology and configuration of the AlN nanorod array after the two-step etching process. First, the formation of smooth and straight facets is enhanced at low pressure and high V/III ratio.[47] Low pressure enhances Al-adatom diffusion, allowing a complete coverage of the AlN nanorod. High V/III ratio reduces the growth rates of both the *c*- and *m*-planes relative to the *a*-plane growth rate, favoring a complete coverage of the AlN nanorod, but also mitigating the growth on the top pyramidal part, which is not favorable for a smooth and straight facet regrowth.[46,47] Second, the use of straight and smooth AlN-etched nanorods prevents the formation of regrowth steps that can be induced by etch damage, especially in these growth conditions where the *m*-plane growth rate is lowered.[47] The small nanorod diameters used in this work allow the formation of *m*-plane facets along the whole height of the nanorod, which is not the case for larger diameters.[47] Finally, the use of a relatively large 1.5 μm pitch allows good gas-phase diffusion of the growth reagents to the base of the nanorods, which ensures that there is no variation in the *m*-plane growth rate along the height of the nanorod.[46]

Following the AlN faceting regrowth step, an AlGaN shell was created by adding 2 sccm of TMGa for 2 min and setting the NH_3 flow rate to 500 sccm (V/III = 1638), with otherwise the same growth conditions, resulting in an approximate thickness of ∼2−3 nm based on the *m*-plane AlN growth rate previously extracted. An AlN cap layer was then grown for 15 min with the same AlN conditions to create an AlGaN/AlN SQW (AlGaN SQW 1). The resulting core−shell structures are displayed in Figure 3a,b. Both SEM and TEM images show straight and smooth sidewalls and a fully formed nanopyramid on the top. No visible extended defects, such as threading dislocations (TDs) or basal stacking faults (BSFs), are observed in the nanorod shown in Figure 3b. The creation of the 130 nm diameter AlN nanorod array has acted to filter the TDs, as shown in Figures 2a and S4, so that zero or at the most one TD is observed in the resulting nanorods after AlN regrowth.[24,25] Any TDs present often bend toward the lateral free surfaces and can be seen as surface pits in Figures 2b and S5. Figure 3c−e displays the aluminum, nitrogen, and gallium concentration, respectively, of the grown core−shell structures as measured by energy-dispersive X-ray (EDX) spectroscopy. Gallium incorporation is observed across the whole height of the nanorod as well as on the semipolar plane.

The optical emission of the AlN/AlGaN/AlN core−shell structures was assessed by room-temperature high-resolution cathodoluminescence (CL) hyperspectral imaging in a low-vacuum SEM (ESEM) and is presented in Figure 4. The intensity map in Figure 4b shows the extracted emission intensity of the SQW between 4.9 and 5.5 eV for a single AlN/AlGaN/AlN core−shell nanorod (Figure 4a). Higher emission intensity arises from the top of the nanorod, at the corners between the semipolar and nonpolar planes, and where regrowth has taken place on the etched planar AlN surface between the nanorods. Indeed, after the two etching steps, hexagonal trenches are created at the base of the nanorods (inset in Figure 1a). Although these do not impact the AlN faceting regrowth step, preferential incorporation seems to occur during the SQW growth. This "parasitic growth" could be suppressed by passivating the AlN bottom *c*-plane with a hydrogen silsesquioxane layer.

Focusing on the nanorod emission characteristics, Figure 4c shows a line spectrum extending from top to bottom of the nanorod (excluding the parasitic emission), and displayed on a log scale. Both the AlN near band edge (NBE) emission and AlGaN SQW emission can be observed along the whole height of the nanorod. The broad AlN NBE emission at 5.8−6.0 eV (207−214 nm) displays a higher intensity on the top semipolar part of the nanorod. The AlN NBE emission range agrees with that reported in the literature at room temperature.[49−51] A lower energy broad emission band is generally observed

DOI: 10.1021/acsami.8b10605
ACS Appl. Mater. Interfaces 2018, 10, 33441−33449

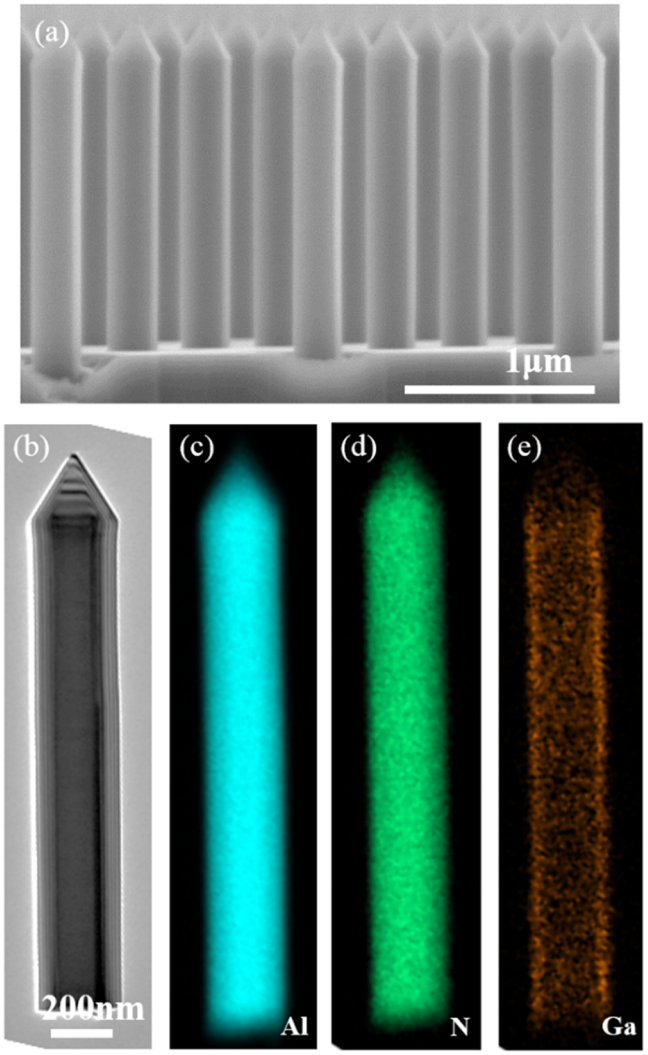

Figure 3. (a) Cross-section SEM and (b) TEM pictures of AlN/AlGaN SQW core−shell structures (AlGaN SQW 1) grown by MOVPE. (c) Al, (d) N, and (e) Ga concentration maps obtained by EDX spectroscopy.

between 2.6 and 4.3 eV for all samples (Figures S6 and S7). The high intensity of the defect luminescence is partly due to the low-vacuum mode in which the CL images were acquired and is not indicative of the quality of the sample (see Supporting Information for further discussion). The defect band, initially observed in the AlN template,[47] could be related to O-complexes and/or Si-complexes and other native defects, such as vacancies.[38,47,52,53] The AlGaN SQW shows two emission energies: one centered around 5.13 eV (242 nm) on both the *m*-plane facets and semipolar facets and a second one centered around 5.22 eV (238 nm) having a higher intensity and localized at the corners between the semipolar and nonpolar nanorod facets. The small energy shift occurring at the corners between the semipolar and nonpolar planes could be due to a change of the surface morphology at the intersection, preferential incorporation of species as a result of strain relaxation at the corners, or from a local change of the QW thickness, similar to that observed for InGaN/GaN core−shell structures.[54,55] Note that the higher intensity could also result from a local change to the QW thickness or enhanced light extraction.

On the basis of the results presented in Figure 4, additional AlGaN/AlN SQW growths have been performed to improve the emission characteristics, such as intensity and uniformity, but also to tune the emission wavelength. Figure 5a−c displays the characteristics obtained at lower growth temperature and higher pressure (AlGaN SQW 2), whereas Figure 5d−f shows the characteristics for an additional increase in TMGa flow rate (AlGaN SQW 3). The SQW thickness can be approximately estimated to be ∼2−3 and ∼10−15 nm, respectively, for AlGaN SQW 2 and 3. More details on the SQW growth conditions are given in the Methods section. Compared to AlGaN SQW 1 (Figure 4b), the intensity map extracted for AlGaN SQW 2 between 5 and 5.7 eV (Figure 5b) suggests an improved intensity of the emission from the nanorod sidewalls to that from the planar *c*-plane. The line spectrum extracted from the top to the bottom of the nanorod in Figure 5c confirms the improvement of the AlGaN SQW emission centered around 229 nm (5.41 eV): it has a similar intensity to the AlN NBE and a good emission uniformity across the whole height of the nanorod. Utilizing a lower growth temperature and higher pressure likely decreased the Al-adatom diffusion, and hence mitigated any preferential incorporation on strain-relaxed surfaces. The lower emission wavelength of the SQW can be explained by Ga desorption during the ramp in temperature between the SQW growth and the AlN cap layer growth.

The increase in TMGa flow rate by a factor of five (AlGaN SQW 3), while keeping all other growth conditions constant, results in a clear red shift of the emission energy range of the SQW from 5−5.7 to 4.4−5 eV (Figure 5e). The intensity is no longer uniform (Figure 5e) with some small differences observed from different parts of the nanorod, with higher intensities at the intersections between the semipolar and nonpolar planes, at intersections between two nonpolar planes (vertical line along the height of the nanorod) and at the bottom of the nanorod. The emission along the height of the nanorod is also no longer uniform with a slight red shift in emission energy from the bottom to the top of the nanorod. The 5-fold increase in TMGa, while keeping the same growth time, is expected to lower the emission energy and increase the growth rate, thus creating a thicker AlGaN layer. As already reported for InGaN/GaN core−shell nanorods,[56,57] a small thickness gradient along the height of the nanorod can lead to a gradual shift of the emission. Additionally, the observation of a higher intensity at the intersections of the planes can also arise from the growth of a thicker layer since it leads to preferential incorporation of species on strain-relaxed regions.[54,55] This preferential incorporation can lead to the formation of a quantum wirelike structure that will enhance the recombination rate and hence the intensity.

Regardless of the small nonuniformity of the emission observed for AlGaN SQW 3, the overall SQW intensity is drastically improved for growth conditions of AlGaN SQW 3. Indeed, while the AlN NBE emission remains more or less at the same intensity (∼10^5 counts) between AlGaN SQW 2 and 3 (respectively, Figure 5c,f), the AlGaN SQW intensity is increased by an order of magnitude in AlGaN SQW 3. Similarly, significant improvement in the nanorod intensity relative to the planar *c*-plane is also observed. This can be clearly observed in Figure 6, which compares for the three AlGaN SQWs the spectra acquired on the *m*-plane nanorod sidewalls (full line) with the one acquired on the planar unpassivated *c*-plane (dashed line). Although the intensity is

DOI: 10.1021/acsami.8b10605
ACS Appl. Mater. Interfaces 2018, 10, 33441−33449

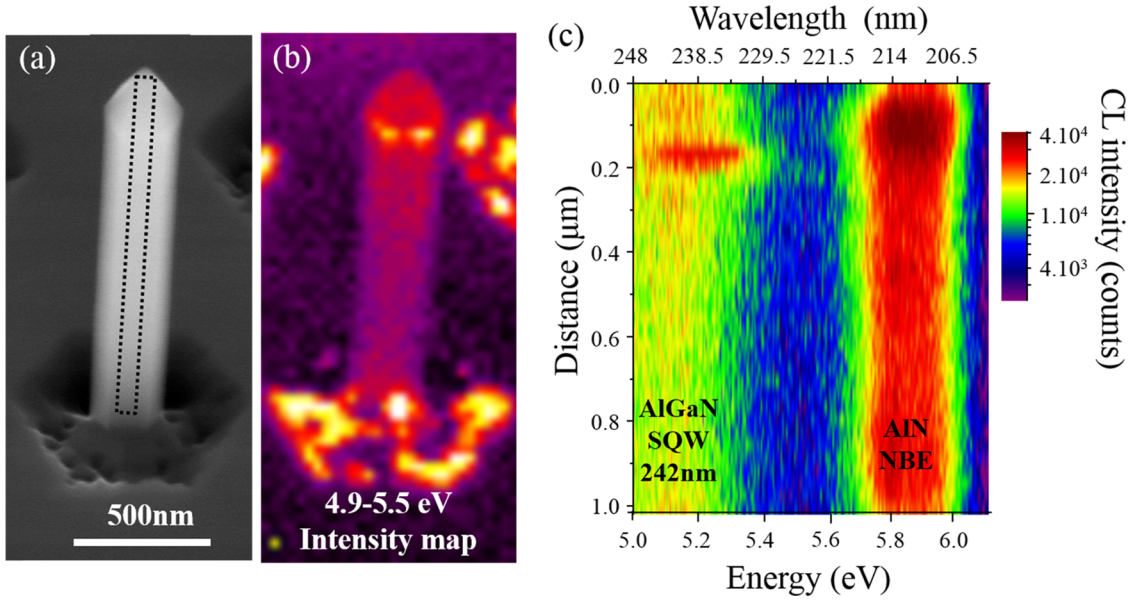

Figure 4. (a) Tilted SEM images of AlGaN SQW 1. (b) Related intensity map extracted over the SQW emission range of 4.9−5.5 eV. (c) Log-scale RT spectral line spectrum extracted along the length of the nanorod displayed in (a) from the region highlighted by the dashed rectangle.

increased by a factor 1.5 for the SQWs emitting at 242 and 229 nm (respectively AlGaN SQW 1 and 2), the enhancement factor reaches 5 for the SQW emitting at 265 nm (AlGaN SQW 3). For all AlGaN SQWs, the enhancement could be attributed to the higher structural quality of the AlN nanorod template compared to the *c*-plane in between, and to a better overlap between the electron and hole wave functions within the nonpolar SQW. In addition, the polarization dependence on substrate orientation should be considered. For *c*-plane growth, polarization switching from light with a dominant polarization of $E\perp c$ to light with a dominant polarization of $E\|c$ occurs when the Al concentration increases. The switch occurs between $x \approx 0.25$ (~300 nm emission)[58,59] and $x \approx 0.8$ (~230 nm)[60] depending on the strain in the QW, its thickness and the internal electric fields.[60,61] For *m*-plane growth, the change in the SQW symmetry results in a modification of the valence sub-bands, which leads to the lowest energy transition being strongly polarized along $E\|c$ for a wide range of Al compositions.[62,63] Hence, the emission is likely to be polarized along $E\|c$ for both the bottom *c*-plane and lateral nanorod *m*-planes, with the latter orientation resulting in less reabsorption due to reduced guiding in the plane of the QW. Further improvement for AlGaN SQW 3 could be due to higher carrier confinement and/or reduced carrier leakage due to the thicker QW. These results demonstrate that optimizing the growth conditions enables tuning of the emission wavelength and significantly improves the intensity while maintaining a high or relatively high emission uniformity from the whole height of the nanorods.

A striking result that is observed in all of the AlGaN SQWs relates to the peak emission wavelength coming from the different planes. As observed in the line spectra extracted along the height of the nanorods in Figure 5c,f and on the CL spectra acquired on both *c*-planes and *m*-planes in Figure 6, no difference in the peak wavelength was observed between different planes. The resulting high uniformity of the emission of the overall core−shell structures, irrespectively of the plane orientation, represents a major advantage compared to visible InGaN/GaN core−shell structures where the indium incorporation is highly sensitive to the plane orientation.[64,65] For visible InGaN/GaN core−shell structures, this generally induces a change of the EL peak emission position as a function of the injection current.[36]

It should be noted that although several electrically injected InGaN/GaN core−shell LEDs emitting in the visible have been demonstrated, there are still further obstacles before devices based on AlGaN/AlN core−shell structures are realized. One major issue is the poor n-type conductivity of the AlN layer forming the core. This could be circumvented by the use of mid to high Al content n-type AlGaN layer for which relatively good carrier density has been reported.[66] Since the hybrid top-down/bottom-up approach can be transferred to any III-nitride template, both binary and ternary alloys, its application to state of the art n-type AlGaN layers represents the most promising solution for electrically injected core−shell structures emitting in the deep UV.

CONCLUSIONS

The paper demonstrates an original and reproducible approach for creating highly uniform and organized arrays of core−shell AlN/AlGaN/AlN nanorods that avoids the difficulties of creating bottom-up nanostructures in the AlGaN materials system. In the combined top-down-etching/bottom-up-growth approach, we employ the recently developed nanolithographic technique of displacement Talbot lithography to create a metal dot etch mask across a full 2 in. wafer via lift off. The successful fabrication of uniform AlN nanorods with smooth vertical facets is then achieved by the sequential use of dry etching, wet etching, and MOVPE regrowth using optimized conditions. This led to large areas of uniform nanorods with an aspect ratio as high as 12. A future reduction of the nanorod pitch from 1.5 to 1 μm with the same nanorod aspect ratio, which we believe is technically feasible with this technique, would lead to a two-time enhancement of the active area compared to planar QWs, thus potentially allowing more efficient LED operation by mitigating droop.

An AlGaN single quantum well (SQW) has been successfully regrown on the AlN nanorods along their entire

DOI: 10.1021/acsami.8b10605
ACS Appl. Mater. Interfaces 2018, 10, 33441−33449

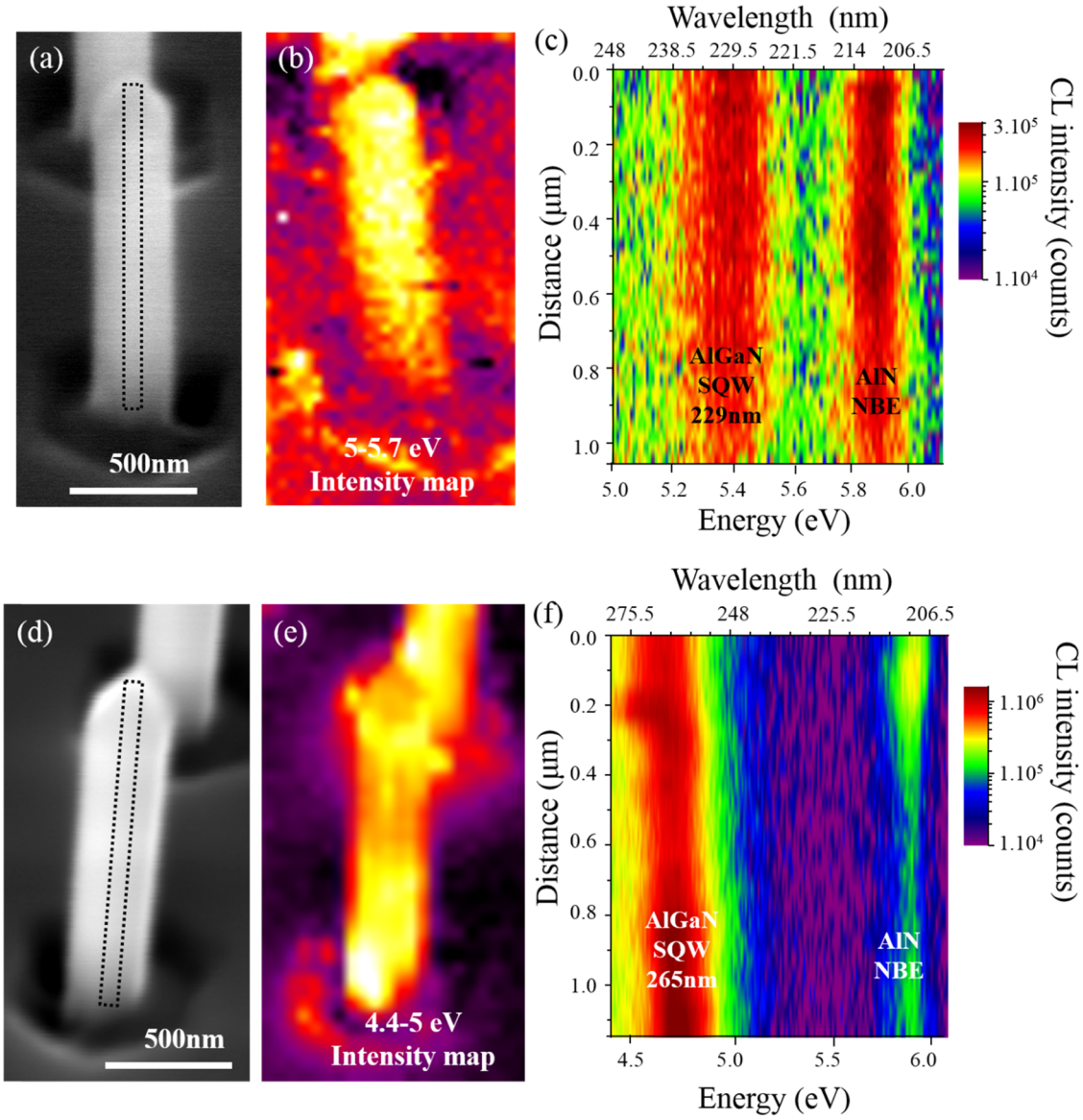

Figure 5. (a) Tilted SEM images of AlGaN SQW 2. (b) Corresponding intensity map extracted over the SQW emission range of 5−5.7 eV. (c) Log-scale RT spectral line spectrum extracted along the length of the nanorod displayed in (a) from the region highlighted by the black dashed rectangle. (d) Tilted SEM images of AlGaN SQW 3. (e) Corresponding intensity map extracted over the SQW emission range of 4.4−5 eV. (f) Log-scale RT spectral line spectrum extracted along the length of the nanorod display in (d) and from a region highlighted by the dashed rectangle.

height, as determined by detailed electron-beam spectroscopic measurements, with a significant improvement of the emission coming from the nonpolar facets compared to the *c*-plane planar growth. Deep UV emission at 229 nm is reported on AlN/AlGaN/AlN core−shell structures for the first time. No facet-dependent alloy incorporation is observed, in contrast to visible-emitting core−shell structures, which will simplify the implementation of these 3D structures into electrically driven devices by allowing a more stable emission wavelength with drive current.

The approach for creating nanostructures that combines top-down-etching with bottom-up growth shows great promise for the fabrication of deep UV LEDs based on core−shell nanostructures due to the flexibility of creating cores with a wide range of $Al_xGa_{1-x}N$ alloy compositions and the controllability of creating regular arrays with a high degree of diameter and height uniformity. Such LEDs will have application, for example, in water and air sterilization.

METHODS

Displacement Talbot Lithography Patterning. Commercial AlN templates (Nanowin) were spin-coated at 3000 rpm with a bottom antireflective layer (BARC) (Wide 30C, Brewer Science) to obtain a layer thickness of 290 nm, followed by a 240 nm layer of positive photoresist (Ultra-i 123, Dow Electronic Materials). We used displacement Talbot lithography (DTL) (PhableR 100, Eulitha) to expose the photoresist with a ∼375 nm laser source through a conventional photomask comprising 800 diameter holes in a hexagonal arrangement with a 1.5 μm pitch. The initial proximity gap was set to 150 μm and the displacement during exposure was 71.2 μm, corresponding to eight Talbot lengths. After exposure, a postexposure bake for 1 min 30 s at 120 °C was applied before development in MF-CD-26. Figure S1 shows the 260 nm diameter openings achieved after the DTL patterning process.

AlN Nanorod Array Fabrication. An electron-beam evaporator was used to deposit 10 nm of Au and 200 nm of Ni on the AlN wafer to create metal masks in the circular opening at the AlN surface. The positive resist and wet-developable BARC was used to create a lift-off

DOI: 10.1021/acsami.8b10605
ACS Appl. Mater. Interfaces 2018, 10, 33441−33449

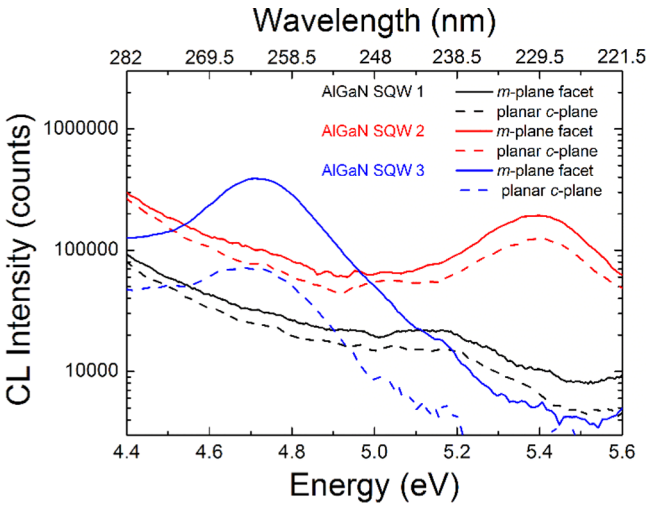

Figure 6. CL spectra acquired for the three AlGaN SQWs showing both emission from the *m*-plane nanorod sidewalls (full line) and also from the *c*-plane material in between the nanorods (dashed line).

profile with MF-CD-26 developer, and the AlN wafer cleaned in a 2 min reactive-ion etching oxygen plasma to remove any BARC residue prior to evaporation. The resulting ~250 nm Au/Ni dots after lift-off are displayed in Figure S2. AlN nanorods were then created using an inductively coupled plasma (ICP) dry etcher (Oxford Instruments System 100 Cobra) using conditions reported previously.[38] Any passivation layer on the slightly undercut nanorod sidewalls (Figure S3a) was then removed in buffered oxide etchant prior for further wet etching in AZ 400K potassium hydroxide-(KOH)-based developer to further smooth and shrink the diameters of the nanorods (Figures 1a and S3b). Finally, the Ni mask was removed in HCl/HNO_3, 3:1.

Faceting Regrowth of AlN Nanorods by MOVPE. The bottom-up regrowth of AlN and AlGaN was carried out in a 1 × 2 inch horizontal Aixtron MOVPE reactor. The employed growth parameters are summarized in Table 1. The growth conditions to satisfy a smooth and straight AlN faceting regrowth follow our previous report,[38] and summarized here: a growth temperature of 1100 °C, a pressure of 20 mbar, 10 sccm in TMAl flow rate, 4000 sccm in NH_3 flow rate (V/III ratio of 30 554), and H_2 as the carrier gas. AlGaN single quantum well (SQW) growth was performed for three different conditions: for AlGaN SQW 1, depicted in Figures 3 and 4, a growth temperature of 1100 °C, a pressure of 20 mbar, 10 sccm in TMAl flow rate, 2 sccm in TMGa flow rate, 500 sccm in NH_3 flow rate (V/III ratio of 1638), and H_2 as the carrier gas; for AlGaN SQW 2, depicted in Figure 5a–c, a growth temperature of 1050 °C, a pressure of 100 mbar, 10 sccm in TMAl flow rate, 2 sccm in TMGa flow rate, 500 sccm in NH_3 flow rate (V/III ratio of 1638), and H_2 as the carrier gas; for AlGaN SQW 3, depicted in Figure 5d–f, a growth temperature of 1050 °C, a pressure of 100 mbar, 10 sccm in TMAl flow rate, 10 sccm in TMGa flow rate, 500 sccm in NH_3 flow rate (V/III ratio of 499), and H_2 as the carrier gas. The AlN cap layer was grown with the same conditions as the AlN faceting regrowth step.

Structural Characterization. Scanning electron microscopy (SEM) was used to monitor the fabrication process and determine the morphology and dimensions of the structures, using a Hitachi S-4300 SEM. The morphology and chemical information of AlGaN/AlN core–shell structures were investigated using a JEOL 2100 200 kV TEM. The core–shell nanorods used for TEM observations were mechanically removed from the wafer and deposited on a carbon grid, hence no mechanical polishing or focused ion beam thinning has been performed.

Optical Characterization. Cathodoluminescence hyperspectral imaging measurements were carried out on the AlGaN/AlN core–shell nanorods at room temperature in a modified FEI Quanta 250 field-emission scanning electron microscope. The electron-beam energy was set to 15.0 keV and the beam current to ~7 nA. A reflecting objective (NA 0.28) with its axis perpendicular to the electron-beam collected the light and focused it on the 50 μm entrance slit of the spectrograph using an off-axis paraboloidal mirror. The spectrograph had a focal length of 125 mm, and the diffracted light from the 600 lines/mm grating was focused onto a cooled electron-multiplying charge-coupled device detector.

■ ASSOCIATED CONTENT

Supporting Information

The Supporting Information is available free of charge on the ACS Publications website at DOI: 10.1021/acsami.8b10605.

Detail on DTL patterning and lift-off to create a hard etch mask and additional SEM images; SEM images comparing nanorod after dry and wet etch; additional TEM images of etched and faceted nanorods; further results and details of the cathodoluminescence characterization (PDF)

■ AUTHOR INFORMATION

Corresponding Author

*E-mail: P.Coulon@bath.ac.uk.

ORCID

Pierre-Marie Coulon: 0000-0002-9120-7554

Gunnar Kusch: 0000-0003-2743-1022

Philip A. Shields: 0000-0003-0517-132X

Present Address

Department of Electronic and Electrical Engineering, University of Bath, Bath BA2 7AY, U.K. (P.-M.C.).

Author Contributions

P.-M.C. conceived the experimental work, supervised by P.A.S. P.-M.C. carried out the nanorod fabrication, MOVPE growth experiment, and SEM characterization. G.K. and R.W.M. performed the CL characterization. All of the authors contributed in analyzing and writing the results.

Notes

The authors declare no competing financial interest.

■ ACKNOWLEDGMENTS

The authors would like to acknowledge financial support of the EPSRC, UK via Grant No. EP/M015181/1, "Manufacturing nano-engineered III-nitrides". This publication is supported by multiple data sets, which are openly available here: https://doi.

Table 1. Growth Parameters Employed for the Different Samples

growth step	temperature (°C)	pressure (mbar)	NH_3 (sccm)	TMAl (sccm)	TMGa (sccm)	V/III ratio
AlN faceting	1100	20	4000	10	0	30 554
AlGaN SQW 1	1100	20	500	10	2	1638
AlGaN SQW 2	1050	100	500	10	2	1638
AlGaN SQW 3	1050	100	500	10	10	499
AlN cap	1100	20	4000	10	0	30 554

DOI: 10.1021/acsami.8b10605
ACS Appl. Mater. Interfaces 2018, 10, 33441–33449

org/10.15125/BATH-00542. We also acknowledge the support of P. Chausse for the DTL patterning and P. Fletcher and the Microscopy and Analysis Suite at the University of Bath for TEM/EDX measurements.

REFERENCES

(1) Anayaogu, K. C.; Ermoshkin, A. A.; Neckers, D. C.; Mejiritski, A.; Grinevich, O.; Fedorov, A. V. Performance of the light emitting diodes versus conventional light sources in the UV light cured formulations. *J. Appl. Polym. Sci.* **2007**, *105*, 803−808.
(2) Morison, W. L. *Phototherapy and Photochemotherapy of Skin Disease*, 3rd ed.; CRC Press, 2018.
(3) Hodgkinson, J.; Tatam, R. P. Optical gas sensing: a review. *Meas. Sci. Technol.* **2013**, *24*, No. 012004.
(4) Xu, Z.; Sadler, B. M. Ultraviolet communications: potential and state-of-the-art. *IEEE Commun. Mag.* **2008**, *46*, 67−73.
(5) Vilhunen, S.; Särkkä, H.; Sillanpää, M. Ultraviolet light-emitting diodes in water disinfection. *Environ. Sci. Pollut. Res.* **2009**, *16*, 439−442.
(6) Würtele, M. A.; Kolbe, T.; Lipsz, M.; Külberg, A.; Weyers, M.; Kneissl, M.; Jekel, M. Application of GaN-based deep ultraviolet light emitting diodes—UV-LEDs—for Water disinfection. *Water Res.* **2011**, *45*, 1481.
(7) Zyara, A. M.; Heinonen-Tanski, H.; Veijalainen, A.-M.; Torvinen, A. UV-LEDs Efficiently Inactivate DNA and RNA Coliphages. *Water* **2017**, *9*, 46.
(8) Kneissl, M.; Rass, J. III-Nitride Ultraviolet Emitters. In *Technology and Applications*; Springer Series in Materials Science; Springer, 2016. Vol. *227*.
(9) Takano, T.; Mino, T.; Sakai, J.; Noguchi, N.; Tsubaki, K.; Hirayama, H. Deep-ultraviolet light-emitting diodes with external quantum efficiency higher than 20% at 275 nm achieved by improving light-extraction efficiency. *Appl. Phys. Express* **2017**, *10*, No. 031002.
(10) Hirayama, H.; Maeda, N.; Fujikawa, S.; Toyoda, S.; Kamata, N. Recent progress and future prospects of AlGaN-based high-efficiency deep-ultraviolet light-emitting diodes. *Jpn. J. Appl. Phys.* **2014**, *53*, No. 100209.
(11) Narukawa, Y.; Ichikawa, M.; Sanga, D.; Sano, M.; Mukai, T. White light emitting diodes with super-high luminous efficacy. *J. Phys. D Appl. Phys.* **2010**, *43*, No. 354002.
(12) Zhao, Y.; Fu, H.; Wang, G. T.; Nakamura, S. Toward ultimate efficiency: progress and prospects on planar and 3D nanostructured nonpolar and semipolar InGaN light-emitting diodes. *Adv. Opt. Photonics* **2018**, *10*, 246.
(13) Martens, M.; Mehnke, F.; Kuhn, C.; Reich, C.; Kueller, V.; Knauer, A.; Netzel, C.; Hartmann, C.; Wollweber, J.; Rass, J.; Wernicke, T.; Bickermann, M.; Weyers, M.; Kneissl, M. Performance Characteristics of UV-C AlGaN-Based Lasers Grown on Sapphire and Bulk AlN Substrates. *IEEE Photonics Technol. Lett.* **2014**, *26*, 342.
(14) Ban, K.; Yamamoto, J.; Takeda, K.; Ide, K.; Iwaya, M.; Takeuchi, T.; Kamiyama, S.; Akasaki, I.; Amano, H. Internal Quantum Efficiency of Whole-Composition-Range AlGaN Multiquantum Wells. *Appl. Phys. Express* **2011**, *4*, No. 052101.
(15) Stampfl, C.; Neugebauer, J.; Van De Walle, C. G. Doping of AlxGa1−xN alloys. *Mater. Sci. Eng., B* **1999**, *59*, 253.
(16) Khan, M. A.; Shatalov, M.; Maruska, H. P.; Wang, H. M.; Kuokstis, E. III−Nitride UV Devices. *Jpn. J. Appl. Phys.* **2005**, *44*, No. 7191.
(17) Nam, K. B.; Li, J.; Nakarmi, M. L.; Lin, J. Y.; Jiang, H. X. Unique optical properties of AlGaN alloys and related ultraviolet emitters. *Appl. Phys. Lett.* **2004**, *84*, 5264.
(18) Taniyasu, Y.; Kasu, M. Surface 210 nm light emission from an AlN p−n junction light-emitting diode enhanced by A-plane growth orientation. *Appl. Phys. Lett.* **2010**, *96*, No. 221110.
(19) Park, J.-S.; Kim, J. K.; Cho, J.; Seonga, T.-Y. Review—Group III-Nitride-Based Ultraviolet Light-Emitting Diodes: Ways of Increasing External Quantum Efficiency. *ECS J. Solid State Sci. Technol.* **2017**, *6*, Q42−Q52.
(20) Huang, M.-F.; Lu, T.-H. Optimization of the Active-Layer Structure for the Deep-UV AlGaN Light-Emitting Diodes. *IEEE J. Quantum Electron.* **2006**, *42*, 820.
(21) Shur, M. S.; Gaska, R. Deep-Ultraviolet Light-Emitting Diodes. *IEEE Trans. Electron Devices* **2010**, *57*, 12.
(22) Khan, A.; Balakrishnan, K.; Katona, T. Ultraviolet light-emitting diodes based on group three nitrides. *Nat. Photonics* **2008**, *2*, 77.
(23) Coulon, P.-M.; Mexis, M.; Teisseire, M.; Jublot, M.; Vennéguès, P.; Leroux, M.; Zúñiga-Pérez, J. Double-polarity GaN micropillars grown by metalorganic vapour phase epitaxy: Cross correlation between structural and optical properties. *J. Appl. Phys.* **2014**, *115*, No. 153504.
(24) Coulon, P.-M.; Alloing, B.; Brändli, V.; Vennéguès, P.; Leroux, M.; Zúñiga-Pérez, J. Dislocation-filtering and polarity in the selective area growth of GaN nanowires by continuous-flow MOVPE. *Appl. Phys. Express* **2016**, *9*, No. 015502.
(25) Wang, G. T.; Li, Q.; Wierer, J. J.; Koleske, D. D.; Figiel, J. J. Top-down fabrication and characterization of axial and radial III-nitride nanowire LEDs. *Phys. Status Solidi A* **2014**, *211*, 748.
(26) Waltereit, P.; Brandt, O.; Trampert, A.; Grahn, H. T.; Menniger, J.; Ramsteiner, M.; Reiche, M.; Ploog, K. H. Nitride semiconductors free of electrostatic fields for efficient white LEDs. *Nature* **2000**, *406*, 865.
(27) Laskar, M. R.; Ganguli, T.; Hatui, N.; Rahman, A. A.; Gokhale, M. R.; Bhattacharya, A. High-resolution X-ray diffraction investigations of the microstructure of MOVPE grown a-plane AlGaN epilayers. *J. Cryst. Growth* **2011**, *315*, 208.
(28) Vennéguès, P.; Chauveau, J. M.; Bougrioua, Z.; Zhu, T.; Martin, D.; Grandjean, N. On the origin of basal stacking faults in nonpolar wurtzite films epitaxially grown on sapphire substrates. *J. Appl. Phys.* **2012**, *112*, No. 113518.
(29) Waag, A.; Wang, X.; Fündling, S.; Ledig, J.; Erenburg, M.; Neumann, R.; Al Suleiman, M.; Merzsch, S.; Wei, J.; Li, S.; Wehmann, H. H.; Bergbauer, W.; Straßburg, M.; Trampert, A.; Jahn, U.; Riechert, H. The nanorod approach: GaN NanoLEDs for solid state lighting. *Phys. Status Solidi C* **2011**, *8*, 2296.
(30) Yun, J.; Shim, J.-I.; Hirayama, H. Analysis of efficiency droop in 280-nm AlGaN multiple-quantum-well light-emitting diodes based on carrier rate equation. *Appl. Phys. Express* **2015**, *8*, No. 022104.
(31) Ryu, H. Y.; Choi, I. G.; Choi, H. S.; Shim, J. I. Investigation of Light Extraction Efficiency in AlGaN Deep-Ultraviolet Light-Emitting Diodes. *Appl. Phys. Express* **2013**, *6*, No. 062101.
(32) Inoue, S.-i.; Tamari, N.; Taniguchi, M. 150 mW deep-ultraviolet light-emitting diodes with large-area AlN nanophotonic lightextraction structure emitting at 265 nm. *Appl. Phys. Lett.* **2017**, *110*, No. 141106.
(33) Bergbauer, W.; Straßburg, M.; Kölper, Ch; Linder, N.; Roder, C.; Lähnemann, J.; Trampert, A.; Fündling, S.; Li, S. F.; Wehmann, H. H.; Waag, A. Continuous-flux MOVPE growth of position-controlled N-face GaN nanorods and embedded InGaN quantum wells. *Nanotechnology* **2010**, *21*, No. 305201.
(34) Coulon, P.-M.; Alloing, B.; Brändli, V.; Lefebvre, D.; Chenot, S.; Zúñiga-Pérez, J. Selective area growth of Ga-polar GaN nanowire arrays by continuous-flow MOVPE: A systematic study on the effect of growth conditions on the array properties. *Phys. Status Solidi B* **2015**, *252*, 1096.
(35) Yeh, T.-W.; Lin, Y.-T.; Stewart, L. S.; Dapkus, P. D.; Sarkissian, R.; O'Brien, J. D.; Ahn, B.; Nutt, S. R. InGaN/GaN Multiple Quantum Wells Grown on Nonpolar Facets of Vertical GaN Nanorod Arrays. *Nano Lett.* **2012**, *12*, 3257−3262.
(36) Jung, B. O.; Bae, S.; Lee, S.; Kim, S. Y.; Lee, J. Y.; Honda, Y.; Amano, H. Emission Characteristics of InGaN/GaN Core-Shell Nanorods Embedded in a 3D Light-Emitting Diode. *Nanoscale Res. Lett.* **2016**, *11*, 215.
(37) Banal, R. G.; Funato, M.; Kawakami, Y. Surface diffusion during metalorganic vapor phase epitaxy of AlN. *Phys. Status Solidi C* **2009**, *6*, 599−602.
(38) Coulon, P.-M.; Kusch, G.; Fletcher, P.; Chausse, P.; Martin, R. W.; Shields, P. A. Hybrid Top-Down/Bottom-Up Fabrication of

DOI: 10.1021/acsami.8b10605
ACS Appl. Mater. Interfaces 2018, 10, 33441−33449

Highly Uniform and Organized Faceted AlN Nanorod Scaffold. *Materials* **2018**, *11*, No. 1140.
(39) Sadaf, S. M.; Zhao, S.; Wu, Y.; Ra, Y. H.; Liu, X.; Vanka, S.; Mi, Z. An AlGaN Core−Shell Tunnel Junction Nanowire Light-Emitting Diode Operating in the Ultraviolet-C Band. *Nano Lett.* **2017**, *17*, 1212.
(40) Belloeil, M.; Gayral, B.; Daudin, B. Quantum Dot-Like Behavior of Compositional Fluctuations in AlGaN Nanowires. *Nano Lett.* **2016**, *16*, 960−966.
(41) Bengoechea-Encabo, A.; Albert, A.; Müller, M.; Xie, M.-Y.; Veit, P.; Bertram, F.; Sanchez-Garcia, M. A.; Zúñiga-Pérez, J.; Mierry, P. D.; Christen, J.; Calleja, E. Selective Area Growth of AlN/GaN Nanocolumns on (0001) and (11−22) GaN/Sapphire for SemiPolar and Non-Polar AlN Pseudo-Templates. *Nanotechnology* **2017**, *28*, No. 365704.
(42) Kim, J.; Choi, U.; Pyeon, J.; So, B.; Nam, O. Deep-Ultraviolet AlGaN/AlN Core-Shell Multiple Quantum Wells on AlN Nanorods via Lithography-Free Method. *Sci. Rep.* **2018**, *8*, No. 935.
(43) Le Boulbar, E. D.; Gîrgel, I.; Lewins, C. J.; Edwards, P. R.; Martin, R. W.; Šatka, A.; Allsopp, D. W. E.; Shields, P. A. Facet recovery and light emission from GaN/InGaN/GaN core-shell structures grown by metal organic vapour phase epitaxy on etched GaN nanorod arrays. *J. Appl. Phys.* **2013**, *114*, No. 094302.
(44) Le Boulbar, E. D.; Edwards, P. R.; Vajargah, S. H.; Griffiths, I.; Gîrgel, I.; Coulon, P.-M.; Cherns, D.; Martin, R. W.; Humphreys, C. J.; Bowen, C. R.; Allsopp, D. W. E.; Shields, P. A. Structural and Optical Emission Uniformity of m-Plane InGaN Single Quantum Wells in Core−Shell Nanorods. *Cryst. Growth Des.* **2016**, *16*, 1907−1916.
(45) Li, C.; Wright, J. B.; Liu, S.; Lu, P.; Figiel, J. J.; Leung, B.; Chow, W. W.; Brener, I.; Koleske, D. D.; Luk, T. S.; Feezell, D. F.; Brueck, S. R. J.; Wang, G. T. Nonpolar InGaN/GaN Core−Shell Single Nanowire Lasers. *Nano Lett.* **2017**, *17*, 1049−1055.
(46) Tian, Y.; Yan, J.; Zhang, Y.; Zhang, Y.; Chen, X.; Guo, Y.; Wang, J.; Li, J. Formation and characteristics of AlGaN-based three-dimensional hexagonal nanopyramid semi-polar multiple quantum wells. *Nanoscale* **2016**, *8*, 11012−11018.
(47) Coulon, P.-M.; Kusch, G.; Le Boulbar, E. D.; Chausse, P.; Bryce, C.; Martin, R. W.; Shields, P. A. Hybrid Top-Down/Bottom-Up Fabrication of Regular Arrays of AlN Nanorods for Deep-UV Core-Shell LEDs. *Phys. Status Solidi B* **2017**, *6*, 599−602.
(48) Li, Q.; Wright, J. B.; Chow, W. W.; Luk, T. S.; Brener, I.; Lester, L. F.; Wang, G. T. Single-Mode GaN Nanowire Lasers. *Optics Express* **2012**, *20*, 17873.
(49) Li, J.; Nam, K. B.; Nakarmi, M. L.; Lin, J. Y.; Jiang, H. X.; Carrier, P.; Wei, S.-H. Band structure and fundamental optical transitions in wurtzite AlN. *Appl. Phys. Lett.* **2003**, *83*, 5163.
(50) Prinz, G. iM.; Ladenburger, A.; Schirra, M.; Feneberg, M.; Thonke, K.; Sauer, R.; Taniyasu, Y.; Kasu, M.; Makimoto, T. Cathodoluminescence, photoluminescence, and reflectance of an aluminum nitride layer grown on silicon carbide substrate. *J. Appl. Phys.* **2007**, *101*, No. 023511.
(51) Taniyasu, Y.; Kasu, M.; Makimoto, T. An aluminium nitride light-emitting diode with a wavelength of 210 nanometres. *Nature* **2006**, *441*, 325−8.
(52) Bryan, Z.; Bryan, I.; Bobea, M.; Hussey, L.; Kirste, R.; Sitar, Z.; Collazo, R. Homoepitaxial AlN thin films deposited on m-plane (1−100) AlN substrates by metalorganic chemical vapor deposition. *J. Appl. Phys.* **2014**, *115*, No. 133503.
(53) Dadgar, A.; Krost, A.; Christen, J.; Bastek, B.; Bertram, F.; Krtschil, A.; Hempel, T.; Bläsing, J.; Haboeck, U.; Hoffmann, A. MOVPE growth of high-quality AlN. *J. Cryst. Growth* **2006**, *297*, 306−310.
(54) Coulon, P.-M.; Hosseini Vajargah, S.; Bao, A.; Le Boulbar, E. D.; Gîrgel, I.; Humphreys, C. J.; Oliver, R. A.; Allsopp, D. W. E.; Shields, P. A.; et al. Evolution of the m-Plane Quantum Well Morphology and Composition within a GaN/InGaN Core−Shell Structure. *Cryst. Growth Des.* **2017**, *17*, 474−482.
(55) Griffiths, J. T.; Ren, C. X.; Coulon, P.-M.; Le Boulbar, E. D.; Bryce, C. G.; Gîrgel, I.; Howkins, A.; Boyd, I.; Martin, R. W.; Allsopp, D. W. E.; Shields, P. A.; Humphreys, C. J.; Oliver, R. A. Structural impact on the nanoscale optical properties of InGaN core-shell nanorods. *Appl. Phys. Lett.* **2017**, *110*, No. 172105.
(56) Müller, M.; Veit, P.; Krause, F. F.; Schimpke, T.; Metzner, S.; Bertram, F.; Mehrtens, T.; Müller-Caspary, K.; Avramescu, A.; Strassburg, M.; Rosenauer, A.; Christen, J. Nanoscopic Insights into InGaN/GaN Core−Shell Nanorods: Structure, Composition, and Luminescence. *Nano Lett.* **2016**, *16*, 5340−5346.
(57) Krause, T.; Hanke, M.; Cheng, Z.; Niehle, M.; Trampert, A.; Rosenthal, M.; Burghammer, M.; Ledig, J.; Hartmann, J.; Zhou, H.; Wehmann, H.-H.; Waag, A. Nanofocus x-ray diffraction and cathodoluminescence investigations into individual core−shell (In,Ga)N/GaN rod light-emitting diodes. *Nanotechnology* **2016**, *27*, No. 325707.
(58) Nam, K. B.; Li, J.; Nakarmi, M. L.; Lin, J. Y.; Jiang, H. X. Unique optical properties of AlGaN alloys and related ultraviolet emitters. *Appl. Phys. Lett.* **2004**, *84*, 5264−5266.
(59) Kolbe, T.; Knauer, A.; Chua, C.; Yang, Z.; Einfeldt, S.; Vogt, P.; Johnson, N. M.; Weyers, M.; Kneissl, M. Optical polarization characteristics of ultraviolet (In)(Al)GaN multiple quantum well light emitting diodes. *Appl. Phys. Lett.* **2010**, *97*, No. 171105.
(60) Banal, R. G.; Funato, M.; Kawakami, Y. Optical anisotropy in [0001]-oriented $Al_xGa_{1-x}N$/AlN quantum wells ($x > 0.69$). *Phys. Rev. B* **2009**, *79*, No. 121308.
(61) Northrup, J. E.; Chua, C. L.; Yang, Z.; Wunderer, T.; Kneissl, M.; Johnson, N. M.; Kolbe, T. Effect of strain and barrier composition on the polarization of light emission from AlGaN/AlN quantum wells. *Appl. Phys. Lett.* **2012**, *100*, No. 021101.
(62) Yamaguchi, A. A. Theoretical investigation of optical polarization properties in Al-rich AlGaN quantum wells with various substrate orientations. *Appl. Phys. Lett.* **2010**, *96*, No. 151911.
(63) Banal, R. G.; Taniyasu, Y.; Yamamoto, H. Deep-ultraviolet light emission properties of nonpolar M-plane AlGaN quantum wells. *Appl. Phys. Lett.* **2014**, *105*, No. 053104.
(64) Gîrgel, I.; Edwards, P. R.; Le Boulbar, E. D.; Coulon, P.-M.; Sahonta, S.-L.; Allsopp, D. W. E.; Martin, R. W.; Humphreys, C. J.; Shields, P. A. Investigation of indium gallium nitride facet-dependent nonpolar growth rates and composition for core−shell light-emitting diodes. *J. Nanophotonics* **2016**, *10*, No. 016010.
(65) Bryce, C.; Le Boulbar, E. D.; Coulon, P.-M.; Edwards, P. R.; Girgel, I.; Allsopp, D. W. E.; Shields, P. A.; Martin, R. W. Quantum well engineering in InGaN/GaN core-shell nanorod structures. *J. Phys. D: Appl. Phys.* **2017**, *50*, No. 42LT01.
(66) Kusch, G.; Mehnke, F.; Enslin, J.; Edwards, P. R.; Wernicke, T.; Kneissl, M.; Martin, R. W. Analysis of doping concentration and composition in wide bandgap AlGaN:Si by wavelength dispersive x-ray spectroscopy. *Semicond. Sci. Technol.* **2017**, *32*, No. 035020.

DOI: 10.1021/acsami.8b10605
ACS Appl. Mater. Interfaces 2018, 10, 33441−33449